

# Universal binding-energy relation for crystals that accounts for surface relaxation

Robin L. Hayes,<sup>1</sup> Michael Ortiz,<sup>2</sup> and Emily A. Carter<sup>1,\*</sup>

<sup>1</sup>Department of Chemistry and Biochemistry, University of California, Los Angeles, California 90095-1569, USA

<sup>2</sup>Engineering and Applied Science Division, California Institute of Technology, Pasadena, California 91125, USA

(Received 18 December 2003; published 19 May 2004)

We present a universal relation for crack surface cohesion including surface relaxation. Specifically, we analyze how  $N$  atomic planes respond to an opening displacement at its boundary, producing structurally relaxed surfaces. Via density-functional theory, we verify universality for metals (Al), ceramics ( $\alpha$ -Al<sub>2</sub>O<sub>3</sub>), and semiconductors (Si). When the energy and opening displacement are scaled appropriately with respect to  $N$ , the uniaxial elastic constant, the relaxed surface energy, and the equilibrium interlayer spacing, all energy-displacement curves collapse onto a single universal curve.

DOI: 10.1103/PhysRevB.69.172104

PACS number(s): 61.50.Lt, 68.35.-p, 71.15.Mb

Macroscopic cohesive theories of fracture often involve empirical postulates on the shape and form of the cohesive law.<sup>1–3</sup> While first principles simulations might be preferable, the typical size of engineering finite element models prohibits their direct application. In order to obtain converged finite element results, the cohesive zone size must be resolved by the mesh; for brittle materials, the cohesive zone size is atomistic, making the calculation prohibitively expensive.<sup>4</sup> Nanometer scale quantum mechanical calculations have provided insight into cracking at the atomic level,<sup>5–8</sup> but their extrapolation to the macroscopic scale is fraught with difficulty. Indeed, orders-of-magnitude mismatch exist between atomistic predictions of cohesive strengths and critical opening displacements<sup>9–11</sup> and measurements of tensile strength in brittle materials obtained from spallation tests,<sup>12</sup> the latter of which are often employed in engineering simulations. The widely used universal binding energy relation (UBER) of Rose *et al.*<sup>13</sup> describes cohesion between rigid surfaces based on atomic scale calculations, but application of the UBER to crack propagation simulations is hampered by its inability to capture the shape and absolute energies of cohesive laws for structurally relaxed surfaces.<sup>6,14–16</sup> Here, we address these difficulties by deriving a coarse-grained cohesive energy relation that accounts for structural relaxation of surfaces and exhibits a material-independent universal form.

Nguyen and Ortiz recently suggested rescaling interlayer potentials to yield macroscopic cohesive laws.<sup>17</sup> Here we extend their work to account for surface relaxation and reconstruction. Specifically, we consider a perfect crystal acted upon by tensile stresses normal to a cleavage plane. The length scales under consideration range from mesoscopic (the dislocation free zone of a metal<sup>18</sup>) to possibly macroscopic (brittle materials); we conservatively denote both scales as mesoscopic. We assume that atomic layers remain planar after deformation, so that the relative displacement of crystallographic layer  $i$  can be described by  $\delta_i$  (the interlayer spacing minus the equilibrium interlayer spacing,  $d$ ) and that the crystal is periodic with a unit cell containing  $N$  atomic layers. We express the total energy per unit area of cleavage plane as

$$E^{\text{tot}} = \phi(\delta_1, \dots, \delta_N) = \sum_{i=1}^N \phi_0(\delta_i) + \phi_1(\delta_1, \dots, \delta_N) \quad (1)$$

subject to the total displacement  $\bar{\delta} = \sum_{i=1}^N \delta_i$ . Here  $\phi_0(\delta) = (1/N)\phi(\delta, \dots, \delta)$  is the local energy per layer of a uniformly expanded crystal and  $\phi_1$  accounts for nonlocal effects across all layers. We hypothesize that  $\phi_0$  dominates bulk crystal behavior, whereas  $\phi_1$  primarily affects surface relaxation at free surfaces.

Assuming the cohesive energy density  $\phi_0(\delta)$  between two layers is convex in the interval  $0 \leq \delta < \delta_0$ , has an inflection point at  $\delta_0$ , is concave for  $\delta > \delta_0$  (i.e., the typical structure of an interatomic potential), and asymptotically approaches twice the *unrelaxed* surface energy,  $2\gamma_0$  (Fig. 1), Nguyen and Ortiz<sup>17</sup> derived the asymptotic limit of the minimized energy  $\bar{\phi}_0(\bar{\delta})$ , the critical opening displacement  $\bar{\delta}_0$ , the cohesive law for the traction  $\bar{t}_0(\bar{\delta})$ , and the peak traction  $\bar{\sigma}_0$ , for the mesoscopic *local* (brittle, defect-free) crystal with structurally unrelaxed free surfaces.

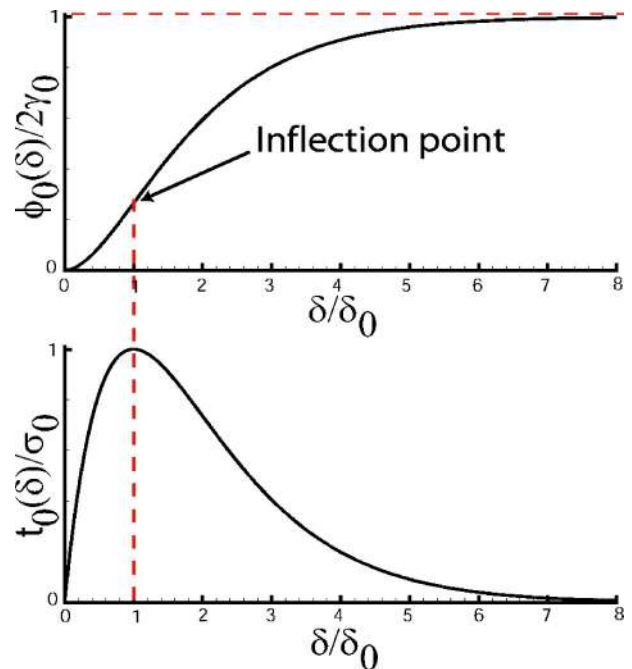


FIG. 1. Generic local interlayer potential and the corresponding traction for separation of rigid surfaces. The critical displacement,  $\delta_0$ , and the critical traction,  $\sigma_0$ , predict the onset of brittle crack formation.

Here, we consider a *matched asymptotic expansion*,<sup>19</sup> in which the local energy,  $\phi_0$ , determines the *outer solution*, and the nonlocal energy,  $\phi_1$ , introduces a singular perturbation and determines the structure of the *inner solution* within narrow boundary layers adjacent to the decohered layers in the local solution. The effect of these boundary layers is to relax the decohered layers and endow them with material-specific structure. The determination of this structure requires consideration of the full energetics of the crystal. Fortunately, in the asymptotic limit, it suffices to assume that the boundary layers surrounding the decohered layers do not overlap, whereupon the previous analysis<sup>17</sup> remains valid with  $\gamma_0$  replaced by the energy of the structurally relaxed surface,  $\gamma_r$ . The asymptotic cohesive energy density now becomes

$$\bar{\phi}(\bar{\delta}) = \min \left\{ \frac{C}{2N} \bar{\delta}^2, 2\gamma_r \right\} = \begin{cases} (C/2N) \bar{\delta}^2, & \text{if } \bar{\delta} < \bar{\delta}_r, \\ 2\gamma_r, & \text{otherwise,} \end{cases} \quad (2)$$

where

$$\bar{\delta}_r = 2\sqrt{\gamma_r N/C} \quad (3)$$

is the critical opening displacement of the structurally relaxed surface and  $C$  is the uniaxial elastic constant. The corresponding mesoscopic cohesive law for the relaxed surface is

$$\bar{t}_r(\bar{\delta}) = \begin{cases} (C/N) \bar{\delta}, & \text{if } \bar{\delta} < \bar{\delta}_r, \\ 0, & \text{otherwise,} \end{cases} \quad (4)$$

and the corresponding peak traction is

$$\bar{\sigma}_r = (C/N) \bar{\delta}_r = 2\sqrt{C\gamma_r/N}. \quad (5)$$

This analysis can be extended to complex Bravais lattices and constrained tangential deformations, if these processes reach equilibrium on the time frame of the crack formation. For example, let  $\eta_i$  be the coordinates of a Bravais sublattice

and let  $\Delta_i$  be the tangential displacement within an atomic layer, constrained to  $\sum_{i=1}^N \Delta_i = 0$  so that the unit cell opens in mode I on average. Then, the extra degrees of freedom ( $\eta_i$  and  $\Delta_i$ ) can be relaxed and the resulting cohesive energy density,  $\phi(\delta_1, \dots, \delta_N)$ , can be minimized as before.

Equation (2) bears a resemblance both to Griffith's criterion for crack propagation and to the expression for the energy release rate of a semi-infinite crack in an elastic strip;<sup>20</sup> however Eq. (2) is derived in a completely different manner. Here our analysis is based on atomistic interplanar potentials without invoking the assumptions of linear elasticity. The preceding analysis shows that the mesoscopic cohesive energy density of a large but finite layer of atomic planes has a *universal*, material-independent, asymptotic structure, Eq. (2), regardless of the specific form of the atomistic binding law. Furthermore,  $\bar{\delta}_r$  and  $\bar{\sigma}_r$  scale as  $\sqrt{N}$  and  $1/\sqrt{N}$ , respectively, potentially bringing the failure criteria ( $\bar{\delta}_r, \bar{\sigma}_r$ ) in line with experimental values with increasing sample thickness. When plotted in terms of the normalized variables,

$$\bar{\delta}^* = \bar{\delta}/(2\sqrt{\gamma_r N/C}) \quad (6)$$

and

$$\bar{\phi}^* = \bar{\phi}/2\gamma_r, \quad (7)$$

the theory predicts that for large  $N$ , *all mesoscopic energy density vs surface separation laws should fall on a single universal curve*, namely, a parabolic arc joining the points (0,0) and (1,1) followed by a horizontal asymptote at 1 [black line in Fig. 2(b)].

To test our theory, we use quantum mechanical calculations [density functional theory (DFT)] to examine three materials exhibiting starkly contrasting behavior. Namely, we consider cleavage along the (111) surfaces of fcc Al, the (0001) surfaces of  $\alpha$ -Al<sub>2</sub>O<sub>3</sub>, and the (100) surfaces of cubic diamond Si. Al is a ductile metal whose (111) surface remains almost bulk-terminated except for a 1% outward ex-

TABLE I. Experimental and DFT material parameters. (Experimental values are in [ ].)

	d [Å] <sup>a</sup>	C [GPa/Å] <sup>b</sup>	$\gamma_r$ [J/m <sup>2</sup> ] <sup>c</sup>	$\delta_0(\bar{\delta}_r)$ [Å] <sup>d</sup>	$\sigma_0(\bar{\sigma}_r)$ [MPa] <sup>e</sup>
(111) fcc Al	2.332 [2.328]	35.3 [52.0]	0.79 [1.18]	0.54 (196)	10900 (161)
(0001) $\alpha$ -Al <sub>2</sub> O <sub>3</sub>	2.189 [2.165]	180.8 [231.4]	1.49 [0.93]	0.55 (123)	47100 (486)
(100) cubic diamond Si	1.365 [1.357]	101.5 [123.5]	1.32 [1.36]	0.57 (195)	28200 (270)

<sup>a</sup>Interlayer separation: Experimental values for Al and Al<sub>2</sub>O<sub>3</sub> at 0 K, Si at 77 K (Ref. 32).

<sup>b</sup>Uniaxial moduli: Experimental values calculated with  $C = (1/d) c_{ijkl} m_i m_j m_k m_l$ ,  $\mathbf{m}$  unit normal to cleavage plane (Ref. 17). Expt.  $c_{ijkl}$  for Al and Al<sub>2</sub>O<sub>3</sub> at 0 K, Si at 77 K (Ref. 32).

<sup>c</sup>Relaxed surface energy:  $W_{ad} = 2\gamma_r$ . Experimental Al extrapolated to 0 K (Ref. 25), Al<sub>2</sub>O<sub>3</sub> empirically extrapolated to 0 K from high  $T$ , so likely underestimated (Ref. 24),  $2 \times 1$  Si from void at 973 K (Ref. 33).

<sup>d</sup>Critical displacement from traditional UBER for unrelaxed surfaces. Values in ( ) from this work, Eq. (3) assuming a 10  $\mu\text{m}$  single crystal.

<sup>e</sup>Critical stress from traditional UBER for unrelaxed surfaces. Values in ( ) from this work, Eq. (5) assuming a 10  $\mu\text{m}$  single crystal.

pansion. When cleaved, the (0001) surface of the brittle ceramic,  $\alpha$ - $\text{Al}_2\text{O}_3$ , undergoes severe inward relaxation of the Al ions by  $\sim 0.7$  Å relative to the bulk termination.<sup>21</sup> The exposed (100) semiconductor Si surface also relaxes inward by 2% relative to the bulk termination, but more importantly, the surface undergoes a  $2\times 1$  reconstruction resulting in rows of dimers.<sup>22</sup>

We use 3D periodic generalized gradient approximation (PW91) DFT calculations implemented within the VASP code.<sup>23</sup> Careful convergence tests using ultrasoft pseudopotentials established kinetic energy cutoffs of 337.8 eV, 337.8 eV, and 200 eV, augmentation charge cutoffs of 553.7 eV, 553.7 eV, and 241.9 eV and Monkhorst-Pack kpoint grids of  $11\times 11\times 3$ ,  $3\times 3\times 1$ , and  $4\times 8\times 1$  for Al,  $\alpha$ - $\text{Al}_2\text{O}_3$ , and Si, respectively. An energy convergence criterion of  $1.0\times 10^{-5}$  eV was used for Al and  $\text{Al}_2\text{O}_3$  while a more strict atomic force criterion of 5 meV/Å was employed for Si. To test the theory, a large number of layers would be advantageous, but the calculations quickly become prohibitive. As a compromise, 12, 6, and 12 layers of Al,  $\text{Al}_2\text{O}_3$ , and Si were used.

The DFT data points for the  $\bar{\phi}^*$  vs  $\bar{\delta}^*$  curve were generated by introducing a separation of size  $\bar{\delta}^*$  between two bulk-terminated atomic layers, fixing the unit cell, and allowing all the ionic positions to relax to their minimum energy configuration. Conceptually, this is equivalent to healing a crack below  $\bar{\delta}_r$  or forming relaxed surfaces beyond  $\bar{\delta}_r$ . To explore differences arising from the reconstructed surfaces, a second series of Si calculations sequentially decreased the introduced separation, using the relaxed configuration from the previous step as the initial configuration. The lowest DFT energy for each  $\bar{\delta}^*$  was used in the subsequent analysis of Si. The unique material renormalization parameters,  $\gamma_r$  and  $C$ , were directly extracted from DFT calculations. The relaxed surface energy is given by  $\gamma_r = (\bar{\phi}(\infty) - \bar{\phi}(0))/2A$ , where  $\bar{\phi}(\infty)$  is the energy of the relaxed ionic positions corresponding to the largest introduced separation and  $A$  is the surface area.  $C$  was extracted from a series of single point energy calculations using the same unit cells as the relaxed surface case, but uniformly expanding the layers in the surface normal direction. Those points in the elastic regime were fit to Eq. (2).

Table I lists calculated parameters and directly comparable experimental values. The interlayer spacings from DFT are reasonable. DFT underestimates  $C$ , but obtains the correct ordering. DFT predictions of  $\gamma_r$ , and consequently the work of adhesion ( $=2\gamma_r$ ), are the correct order of magnitude. The deviations in  $\gamma_r$  are likely due to empirical extrapolation from high  $T$  to 0 K;<sup>24,25</sup> experimental surface energies are notoriously difficult to measure.  $\delta_0$  and  $\sigma_0$  are the critical separation and stress for the traditional UBER model (rigid surfaces, no renormalization); these values are orders of magnitude too small and too large, respectively. For comparison, we also give renormalized, structurally relaxed  $\bar{\delta}_r$  and  $\bar{\sigma}_r$  in parentheses, assuming a 10  $\mu\text{m}$  thick crystal. These values are more in line with expected values from an appropriate experiment; note the orders of magnitude

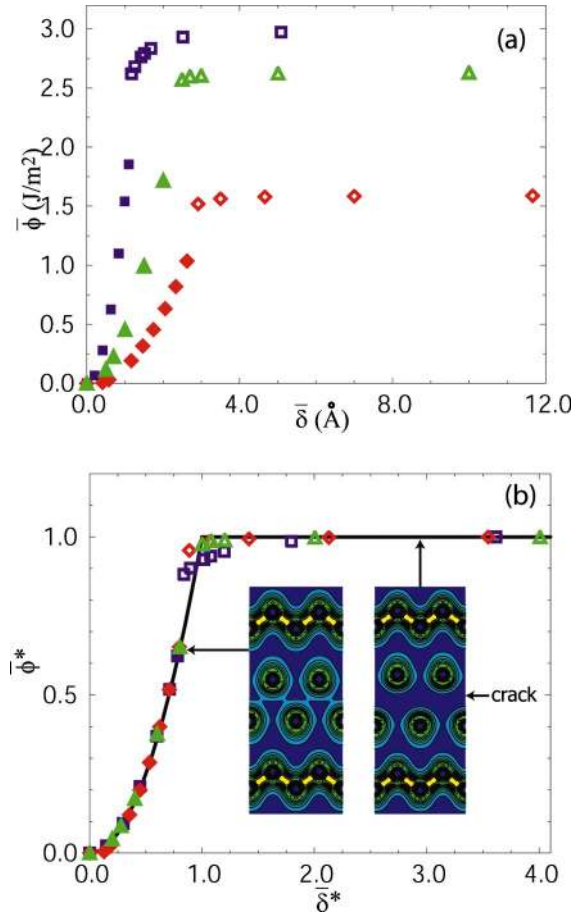


FIG. 2. (Color) The absolute (a) and renormalized (b) energy-displacement DFT data, with the latter collapsing to a universal curve. (111) fcc Al ( $\blacklozenge$ ), (0001)  $\alpha$ - $\text{Al}_2\text{O}_3$  ( $\blacksquare$ ), and (100) cubic diamond Si ( $\blacktriangle$ ) are the DFT data. For filled symbols, the crack heals; for open symbols, the crack remains. (b) The universal curve predicted by Eq. (2) (black line) and the DFT data are renormalized by  $\bar{\phi}^* = \bar{\phi}/2\gamma_r$  and  $\bar{\delta}^* = \bar{\delta}/(2\sqrt{\gamma_r N/C})$ . The inset of rigidly separated Si shows the electron density slice through the surface Si for introduced cracks leading to crack healing ( $\bar{\delta}^* < 1$ ) and crack formation ( $\bar{\delta}^* > 1$ ) upon relaxation. Only when the initial electron density bridges the crack does it heal.<sup>6</sup> Yellow (blue) signifies high (low) electron density.

changes. The ideal experimental comparison for  $\bar{\delta}_r$  and  $\bar{\sigma}_r$  would involve defect-free, brittle, single crystals subject to a uniaxial tensile load on a specific surface orientation conducted near 0 K. Such measurements have not, indeed perhaps cannot, be performed. It is well known that internal flaws and surface cracks in samples produce large variations in fracture strength.<sup>26</sup> Typical experimental tensile  $\bar{\sigma}_r$  values for room temperature specimens of unknown grain size and orientation are 40–50 MPa, 150–500 MPa, and 200–7000 MPa for Al,<sup>27</sup>  $\text{Al}_2\text{O}_3$ ,<sup>28,29</sup> and Si,<sup>30,31</sup> respectively. Since Al is ductile, we expect poor agreement. Only when the values are renormalized as we have outlined do they fall in the experimentally observed range.

Figure 2 shows absolute and renormalized DFT energies of the relaxed surfaces compared to the proposed universal

scaling law for relaxed surfaces. Figure 2(a) illustrates the disparity in intrinsic properties of metal vs ceramic vs semiconductor, while Fig. 2(b) shows that except for the region near (1,1), *all the renormalized DFT data for these three distinctly different materials fall on the same universal curve.* That all the complexities of quantum mechanics, including the long-range interactions between the atoms, should reduce to this simple universal law is truly remarkable. At a fundamental level, we conclude that *all sufficiently large ensembles of planes of atoms subject to a prescribed opening displacement at its boundary behave the same, regardless of material type: in the absence of dislocations, they uniformly expand elastically until they form two structurally relaxed surfaces.* In practice, approximately 10 atomic planes are usually sufficient to reach the asymptotic limit.

This universal law provides a general analytic form for efficiently representing the results from first principles calculations of cohesive behavior. Indeed, it suggests that only three parameters ( $d$ ,  $C$ , and  $2\gamma_r$ ) need be calculated, from which the entire cohesive behavior can be reconstructed, at a

considerable savings in computational cost. Lastly, because the law represents the response of a large but finite number of atomic layers, it provides the means to bridge scales from atomistic to mesoscopic in complex, large-scale finite element simulations.

In closing, some of the limitations for this approach and deviations from the universal curve should be carefully noted. The downward curvature in data near (1,1) is due to finite sample size as well as metastability. The model is based on energy minimization and therefore metastable states are not accounted for. For example, during cyclic loading, the opening and healing traction-separation curves may be different, an effect that is not captured by the theory.

We are grateful to W. Curtin for many useful discussions and suggestions and E. Jarvis for performing the  $\text{Al}_2\text{O}_3$  calculations. This work has been supported by a DoD-MURI grant through Brown University's MURI Center for the "Design and Testing of Materials by Computation: A Multi-Scale Approach."

\*Corresponding author. Email address: eac@chem.ucla.edu.

<sup>1</sup>D. S. Dugdale, J. Mech. Phys. Solids **8**, 100 (1960).

<sup>2</sup>G. I. Barenblatt, Adv. Appl. Mech. **7**, 55 (1962).

<sup>3</sup>J. S. Langer and A. E. Lobkovsky, J. Mech. Phys. Solids **46**, 1521 (1998).

<sup>4</sup>G. T. Camacho and M. Ortiz, Int. J. Solids Struct. **33**, 2899 (1996).

<sup>5</sup>U. V. Waghmare, E. Kaxiras, and M. S. Duesbery, Phys. Status Solidi B **217**, 545 (2000).

<sup>6</sup>E. A. A. Jarvis, R. L. Hayes, and E. A. Carter, ChemPhysChem **2**, 55 (2001).

<sup>7</sup>A. Van der Ven and G. Ceder, Phys. Rev. B **67**, 060101 (2003).

<sup>8</sup>R. Wu, A. J. Freeman, and G. B. Olson, Science **265**, 376 (1994).

<sup>9</sup>A. G. Evans, J. W. Hutchinson, and Y. Wei, Acta Mater. **47**, 4093 (1999).

<sup>10</sup>T. Hong, J. R. Smith, and D. J. Srolovitz, Acta Metall. Mater. **43**, 2721 (1995).

<sup>11</sup>K. Gall, M. F. Horstemeyer, M. Van Schilfgaarde, and M. I. Baskes, J. Mech. Phys. Solids **48**, 2183 (2000).

<sup>12</sup>D. E. Grady and M. E. Kipp, *High-Pressure Shock Compression of Solids* (Springer-Verlag, Berlin, 1993), pp. 265–322.

<sup>13</sup>J. H. Rose, J. R. Smith, and J. Ferrante, Phys. Rev. B **28**, 1835 (1983); T. Hong, J. R. Smith, D. J. Srolovitz, J. G. Gay, and R. Richter, *ibid.* **45**, 8775 (1992).

<sup>14</sup>A. Banerjee and J. R. Smith, Phys. Rev. B **37**, 6632 (1988).

<sup>15</sup>D. J. Siegel, L. G. Hector, Jr., and J. B. Adams, Phys. Rev. B **65**, 085415/1 (2002).

<sup>16</sup>J. R. Smith, G. Bozzolo, A. Banerjee, and J. Ferrante, Phys. Rev. Lett. **63**, 1269 (1989).

<sup>17</sup>O. Nguyen and M. Ortiz, J. Mech. Phys. Solids **50**, 1727 (2002).

<sup>18</sup>V. Tvergaard, J. Phys. IV **8**, 391 (1998); J. Mech. Phys. Solids **6**, 1007 (1997).

<sup>19</sup>C. M. Bender and S. A. Orszag, *Advanced Mathematical Methods for Scientists and Engineers* (McGraw-Hill, New York, 1978), pp. 417–483.

<sup>20</sup>J. R. Rice, in *Fracture*, edited by H. Liebowitz (Academic, New York, 1968).

<sup>21</sup>E. A. A. Jarvis, A. Christensen, and E. A. Carter, Surf. Sci. **487**, 55 (2001).

<sup>22</sup>K. Hata, S. Yoshida, and H. Shigekawa, Phys. Rev. Lett. **89**, 286104 (2002).

<sup>23</sup>G. Kresse and J. Furthmüller, Comput. Mater. Sci. **6**, 15 (1996).

<sup>24</sup>S. K. Rhee, J. Am. Ceram. Soc. **55**, 300 (1972).

<sup>25</sup>W. R. Tyson and W. A. Miller, Surf. Sci. **62**, 267 (1977).

<sup>26</sup>S. M. Hu, J. Appl. Phys. **53**, 3576 (1982).

<sup>27</sup>W. H. Cullberry, *ASM Metals Handbook: Volume 2 Properties and Selection: Nonferrous Alloys*, 9th ed. (American Society for Metals, Metals Park, 1979), p. 715.

<sup>28</sup>R. G. Munro, J. Am. Ceram. Soc. **80**, 1919 (1997).

<sup>29</sup>J. J. Mecholkhy, Jr. and S. R. Powell, Jr., *Fractography of Ceramic and Metal Failures* (ASTM, Philadelphia, 1982), pp. 19, 42.

<sup>30</sup>J. S. Ward, N. C. Woolsey, and R. R. Whitlock, Appl. Phys. Lett. **61**, 651 (1992).

<sup>31</sup>S. M. Hu, J. Appl. Phys. **53**, 3576 (1982).

<sup>32</sup>G. Simmons and H. Wang, *Single Crystal Elastic Constants and Calculated Aggregate Properties: A Handbook* (MIT, Cambridge, MA, 1971), pp. 6, 85, 146.

<sup>33</sup>D. J. Eaglesham *et al.*, Phys. Rev. Lett. **70**, 1643 (1993).